Active control of jet mixing

C.C.L. Yuan, M. Krstić and T.R. Bewley

Abstract: A control law to improve jet flow mixing is presented. The control law employs a pair of actuators at the jet nozzle exit that act on the shear layers near the corners by blowing and subtracting fluid in an anti-symmetric fashion and a sensor downstream or at the nozzle exit with a time delay that measures the pressure difference across the nozzle diameter. A 2-D jet flow is numerically simulated along with massless/mass particles and a passive scalar. The mixing enhancement produced by these controllers is demonstrated visually by snapshots of the vorticity, streaklines, particle distribution and scalar field. Probability function for the particles and the scalar field are constructed, which serve as an index of mixing quality and the effectiveness of the controllers. This closed-loop control law successfully alters the jet flow and improves the mixing of particles with mass and passive scalar.

1 Introduction

Jet flow has been thoroughly studied through theory [1], experiment [2-5] and numerical simulations [6]. Three regions were observed to develop in experiments: (i) the near field; (ii) the transition field; and (iii) the far field. In the near field, two shear layers develop separately with a near-constant centreline streamflow direction velocity. Shear layers appear in the transient field as the jet flow starts to enter the fully developed region. Self-similar profiles are observed in the far field where the mean velocity profiles experience a linear growth of the jet width and a linear decay of the square-of-centreline velocity. The mean stream direction velocity profiles are observed to have a similar bell-shape in all three regions with a smaller centreline velocity and a wider width further downstream. A large number of unstable modes have been observed in the thin shear layers close to the nozzle whereas only the first helical mode has been observed in the fully developed jet at some distance from the end of the potential core [7]. Well developed parabolic velocity profiles at the nozzle exit lead to the initial dominance of the sinuous mode, i.e. the first helical mode of instability [8]. The simulation results of a jet flow without a controller performed in this study closely coincide with the above observations.

The enhancement of jet flow mixing is frequently desirable in many engineering applications. For instance a well mixed air/fuel mixture can improve the overall combustor performance by increasing the combustion efficiency, reducing combustion instability and undesired emissions. Stealth plays a crucial role in the survivability of a warplane. A ground attack plane normally flies at low altitude and thus places it in danger of being tracked by an infrared-homing anti-air missile, e.g. the lightweight stinger missile. The main source of infrared signature is at the jet

nozzle exit, and this can be significantly reduced by an efficient mixing mechanism to quickly disperse the hot gases. A lighter and cheaper material can reduce the manufacturing cost of the lift flap of a C-17, provided that jet exhaust mixing is used to reduce thermal stresses [9].

Many different techniques have been studied to amplify or to excite the unstable modes of a jet flow to increase the mixing quality. Several configurations of static tabs at the jet nozzle exit have been experimentally and numerically examined [2]. Non-circular jets have also received considerable attention and have been thoroughly studied. The results of the experimental and numerical studies on non-circular, rectangular, square and elliptic, nozzle jets can be found in a survey by Gutmark and Grinstein [10]. In addition to these passive methods, different configurations of secondary jets have also been studied. Fuel has been injected at a constant frequency through circumferential holes parallel to the main air jet at the exit plane to obtain soot reduction and more energy release in [11]. Highamplitude low-mass flux-pulsed slot jets blowing normal to the shear layers of the main jet near the nozzle exit plane have been examined experimentally in [12] and numerically in [9]. These transverse jets with constant pulsating frequencies effectively excite the unstable modes and thus significantly alter the development of jet flows. Lardeau et al. [13] have simulated two auxiliary jets, one with and one without constant pulsating frequencies being injected into the main jet with an impinging angle of 45°, and successfully reduced the jet potential core and spread of the jet expansion. MEMS-based micro-flap actuators distributed along a round nozzle have also been employed successfully for the (open-loop) control of a jet flow by Suzuki et al. [14].

The control methods studied in these previous works are either passive or open-loop in nature. A closed-loop control law will be developed in this study to continuously monitor the jet flow parameter and update the actuator on-line so that the mixing quality can be improved. To the best of the authors' knowledge, this is the first attempt to control jet flow mixing using a closed-loop control law.

2 Numerical setup and technique

The equations governing the jet flow in the present case are non-dimensionalised incompressible Navier-Stokes

© IEE, 2004

IEE Proceedings online no. 20041053

doi: 10.1049/ip-cta:20041053

Paper first received 17th September 2003 and in revised form 23rd July 2004

The authors are with the Department of Mechanical and Aerospace Engineering, University of California at San Diego, La Jolla, CA 92093-0411, USA

equations and the continuity equation (in primitive variables):

$$\frac{\partial u_i}{\partial t} + \frac{\partial u_i u_j}{\partial x_i} = -\frac{\partial p}{\partial x_i} + \frac{1}{Re_D} \frac{\partial^2 u_i}{\partial x_i^2} \tag{1}$$

$$\nabla \cdot \boldsymbol{u} = 0 \tag{2}$$

where u_i is the velocity, $\mathbf{u} = (u_1, u_2)$ is the velocity vector, p is pressure field, x_i is the spatial coordinate, and the subscripts i and j represents the spatial direction, '1' is for the streamflow direction and '2' is for the normal direction. The Reynolds number Re_D is based on the jet nozzle diameter D and the centreline velocity at nozzle inlet U_0 . The governing equations, (1) and (2), are used to simulate a spatially evolving jet flow in the computational domain consisting of a jet nozzle with dimensions of 2×1 and an open field with dimensions of 50×40 . All the units are normalised by the nozzle diameter D. The computational domain is shown in Fig. 1. The numerical method used in this research was developed for a backward facing step simulation [15] and a boundary control problem of channel flow [16], and is modified for the current geometry. Therefore, it will be stated here with only a minimal explanation, however, a detailed derivation of this numerical scheme can be found in [15].

The origin of the coordinate system is at the centre of the nozzle exit plane. In the nozzle, the grids are equispaced in the streamflow direction, and stretched in the normal direction with a hyperbolic tangent function. In the open field, a 1-D stretching formula [17] is adapted for the streamflow distribution; in the normal direction, the grid lines in the jet core are equal to the ones in the nozzle, and are distributed using the same 1-D stretching formula otherwise. This stretching formula gives a smooth transition from the finer grids used near the walls and around the shear layers to the coarser grids used in the far field. The total grid numbers are 201 \times 175 in the open field and 11 \times 15 in the nozzle. Sampled grid lines are also illustrated in Fig. 1. A finite-difference scheme is used for the spatial derivatives. Whereas the interior nodes use a second-order accurate central-difference scheme, the boundary nodes use a second-order inward-biased scheme to keep the overall accuracy second-order in space. The primitive variables namely the pressure at the cell centre and the velocities at the grid lines are stored in a staggered grid. The momentum equations are evaluated at the corresponding velocity nodes, and the continuity equation is enforced at the pressure node.

The illustration of a staggered grid can also be found in Fig. 1. Note that the half-grid lines are exactly located at the midpoint between primary grid lines, thus the central-difference approximations of the spatial derivatives across the half-grid lines are exactly second-order accurate. However, the primary grid lines are not located exactly halfway between half-grid lines because of a non-uniform grid distribution, and the differentiations across these primary grid lines are thus not fully second-order accurate. Therefore, the overall accuracy in space is only quasi-second-order accurate even when the second-order preservation formula for velocity interpolation to adjacent grids is used.

A fine resolution near the solid walls and around the shear layers is necessary to resolve the large velocity gradient. The minimum grid spacing is 0.19 in the streamflow direction and 0.04 in the normal direction, and the ratio of the maximum to the minimum grid spacing is 4.71 and 23.29 in the streamflow direction and normal direction, respectively. The grid distribution in the normal direction severely limits the time step, and therefore it is preferred to compute the derivatives in the normal direction implicitly whereas the derivatives in the streamflow direction are treated explicitly. This leads to a hybrid time integration scheme using a low storage third-order Runge-Kutta scheme for the explicitly treated terms and a second-order Crank-Nicholson scheme for the implicitly treated terms, respectively (see [15, 16, 18] for further information). The overall accuracy in time is thus second-order.

The discretised Navier-Stokes equations take the form:

$$\frac{u_i^k - u_i^{k-1}}{\Delta t} = \beta_k [B(\boldsymbol{u}^k) - B(\boldsymbol{u}^{k-1})] - 2\beta_k \frac{\delta p^k}{\delta x_i} + \gamma_k A(\boldsymbol{u}^{k-1}) + \zeta_k A(\boldsymbol{u}^{k-2})$$
(3)

$$A(u_i) = v \frac{\delta^2 u_i}{\delta x_1^2} - \frac{\delta u_1 u_i}{\delta x_1}$$
 (4)

$$B(u_i) = v \frac{\delta^2 u_i}{\delta x_2^2} - \frac{\delta u_2 u_i}{\delta x_2}$$
 (5)

where β , γ and ζ are the coefficients of the third-order Runge-Kutta scheme, $A(u_i)$ and $B(u_i)$ are the explicit and implicit operator respectively, and $v = 1/Re_D$ is the normalised kinematic viscosity. The superscript and subscript k represents the Runge-Kutta substep, where k = 0 is at time step n and k = 3 is at time step n + 1.

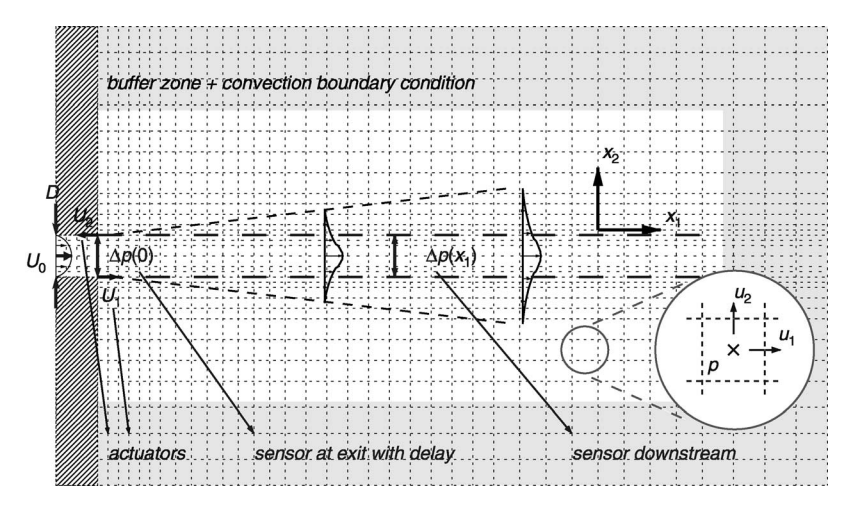


Fig. 1 Computational domain, sampled grid lines, staggered grid illustration, and locations of sensors and actuators

A no-slip condition is applied along all the solid walls. The inflow condition at the inlet of the jet nozzle is a constant parabola for the stream direction velocity with a unit centreline velocity $U_0=1$, and it is a still field for the transverse velocity $u_2=0$. This inflow boundary condition gives us a constant mass flux throughout the computation process. In order to pass the vortical structure through the computation domain smoothly, a convection boundary condition is used along the open boundaries in the open field:

$$\frac{\partial u_i}{\partial t} + U_{\rm con} \frac{\partial u_i}{\partial \mathbf{n}} = 0 \tag{6}$$

where $U_{\rm con}$ is a convection velocity and is chosen to be half of U_0 in the streamflow direction and a quarter of U_0 in the normal direction, and \mathbf{n} is the direction normal to the boundary. This convection boundary condition is computed at full time step by a forward-in-time inward-in-space scheme and is interpolated for each Runge-Kutta substep. To further decrease the non-physical effect of the fictitious boundary of the computation domain, a buffer zone of length ten is inserted in each open boundary. A damping term based on the computed boundary condition is added to the right-hand side of the discretised Navier-Stokes equation, (3). These extra damping terms in the overlap of the buffer zones along the streamflow and normal directions are calculated by a weighted ratio of the distance from two boundaries.

Equation (3) is advanced in time by a fractional step method; a non-divergence free-velocity field is solved first and then this is projected onto a solenoidal field by a pressure update. In order to treat the implicit and explicit terms in a single framework, we have implemented a hybrid Runge-Kutta/Crank-Nicolson technique. The complete Runge-Kutta substep is now written out (in order of actual computation sequence) as follows:

$$\{\boldsymbol{I} - B(\hat{\boldsymbol{u}})\}\hat{\boldsymbol{u}} = \Delta t \{\boldsymbol{u}^{k-1} - \beta_k [B(\boldsymbol{u}^{k-1}) + 2\nabla p^k] + \gamma_k A(\boldsymbol{u}^{k-1}) + \zeta_k A(\boldsymbol{u}^{k-2})\}$$
(7)

$$\nabla^2 \phi = \frac{1}{2\beta_k \Delta t} \nabla \cdot \hat{\boldsymbol{u}} \tag{8}$$

$$\boldsymbol{u}^k = \hat{\boldsymbol{u}} - 2\beta_k \Delta t \nabla \phi \tag{9}$$

$$p^k = p^{k-1} + \phi \tag{10}$$

where $\hat{\boldsymbol{u}}$ is the intermediate velocity field which is not solenoidal, \boldsymbol{I} is the identity matrix and ϕ is the pressure update. Equation (7) is the result of an implicit Crank-Nicolson scheme, and is solved through a tridiagonal system solver. To solve the pressure update, a Poisson solver implementing LU-decomposition is used to solve the Poisson equation, (8); the singularity of this matrix generated by the Poisson equation is removed by prescribing the reference value of zero at the last cell (N_{x_1}, N_{x_2}) in the open field. The divergence is computed after each full time step to ensure a solenoidal field.

In order to monitor the flow evolution, massless particles are introduced to simulate the passive tracer. The positions of these massless particles are governed by the equation dx/dt = u, where x is the position vector of the particle, and u is the velocity vector of the flow fluid at the same point. Streaklines are constructed from the connection between these particles released from the same insertion point. Particles with mass are also injected into the jet to examine

the effectiveness of the control action in a gas-particle jet flow. The particle-particle interaction is neglected due to a large particle spacing. The Basset–Boussinesq–Oseen equation, the governing equation of particle evolution, can be justifiably simplified for gas-particle flow with a very small density ratio between the carrier phase and the discrete phase $(\rho_{\rm f}/\rho_{\rm p} \leq 10^{-3})$ and with the assumption of one-way coupling that only the carrier phase has influence on the particle but not *vice versa* [19]. Thus, the particles are governed by these non-dimensionalised motion equations:

$$\frac{d\mathbf{v}}{dt} = \frac{f}{St}(\mathbf{u} - \mathbf{v}) \tag{11}$$

$$\frac{d\mathbf{x}}{dt} = \mathbf{v} \tag{12}$$

where \mathbf{v} is the particle velocity, $f=1+0.15Re_{\rm p}^{0.687}$ is a correction factor which is a function of the particle relative Reynolds number $Re_{\rm p}=(d_{\rm p}|\mathbf{u}-\mathbf{v}|)/v$, $d_{\rm p}$ is the particle diameter, v is the kinematic viscosity of the flow, and St is the particle Stokes number which is the ratio of the particle's momentum response time to the flow field characteristic time. By definition, a larger Stokes number represents a larger or heavier particle, and a smaller or lighter particle has a smaller Stokes number. Three different Stokes numbers, 0.1, one, and ten, are simulated to examine the response of light, medium and heavy particles to the control action. The particles are fed into the flow at the jet exit plane with normal coordinates y=0 and ± 0.5 every time step, and (11) and (12) are advanced in time by the third-order Runge–Kutta scheme.

In addition to the streaklines and particles with mass, an evolution equation of a passive scalar *S* is also simulated:

$$\frac{\partial S}{\partial t} + \frac{\partial u_j S}{\partial x_j} = \frac{1}{Re_D} \frac{1}{Sc} \frac{\partial^2 S}{\partial x_i^2}$$
 (13)

where Sc is the Schmidt number defined as the ratio of the fluid kinematic viscosity to the scalar's molecular diffusivity and it is set to unity in this study. That this scalar is 'passive' means that the scalar's evolution is influenced by the flow, but that the scalar itself does not have any influence on the flow. The evolution of such a passive scalar provides a useful indicator for mixing in many practical applications, such as combustion studies assuming fast kinetics [6]. Since the scalar field has no influence on the velocity field, the explicit Runge-Kutta scheme is also used to advance (13) in time, as in the particle evolution equations. The scalar field is calculated on the pressure node, and the first-order upwind scheme is used for the spatial derivatives of the convection terms in (13). The scalar field has a highest possible value of one in the nozzle throughout the whole simulation, and a lowest possible value of zero at the open boundaries initially. The convection boundary condition is used. The details of how to advance particle and scalar fields in time are contained in [18].

3 Control strategy

Parekh *et al.* [12] demonstrated tremendous increases in mixing by exciting the flapping mode which is the dominant mode in a low Reynolds number jet flow. This is accomplished by exciting the jet shear layer adjacent to the jet nozzle exit with pulsed fluidic actuators.

In [20] and [21], an active feedback control was applied to excite the instability mechanisms in a 2-D channel flow and a 3-D pipe flow. Mixing was considerably enhanced

with an extremely small control effort by applying a carefully designed closed-loop boundary control law. Decentralised wall-normal suction and blowing was used for actuation with the pressure difference between opposite points on the wall for sensing. The advantage of this feedback control law is its simplicity: a static output-feedback law and a zero net mass flux.

A similar feedback control law is now adapted for jet flow mixing. The controller consists in a pair of actuators acting in the streamflow direction at the jet lips in an antisymmetric fashion $U_1(t) = -U_2(t)$, and a sensor measuring the pressure difference across the nozzle diameter Δp $(x_1, t-\tau)$ $(=p_{y=-0.5}-p_{y=+0.5})$. The control laws are depicted in Fig. 1 and written out for a configuration of a sensor downstream and a sensor at the nozzle exit with time delays, respectively:

$$U_1(t) = K\Delta p(x_1, t) \tag{14}$$

$$U_1(t) = K\Delta p(0, t - \tau) \tag{15}$$

where K is the feedback gain, and τ is the time delay. The control law is computed at each time step and kept constant through a full time step. The saturation of the actuator magnitude is set to the maximum centreline velocity at the nozzle inlet U_0 , and the actuator change rate is saturated at $0.2U_0$ between time steps. The net mass flux introduced by these controllers is kept at zero by injecting and subtracting the same amount of mass.

The control laws (14) and (15) both use delayed pressure measurements, the latter with a temporal delay and the former with spatial delay. The effect of both is similar and the amount of delay applied affects the damping of the dominant (flapping) mode of vortex shedding as well as the frequencies of additional unstable modes that become excited. An optimal level of delay exists, as will be illustrated in subsequent Sections. Whereas the spatial delay (14) is intuitively clear (sufficiently far downstream vortex shedding is sufficiently developed so that measurements of the flow perturbation can be used to amplify it by control) the temporal delay (15) is physically less clear but it is physically implementable because a non-intrusive pressure sensor can be placed at the nozzle. In summary, the implementable temporal delay emulates the effect of the intuitive spatial delay.

More than from any other source, the motivation for the feedback strategies (14) and (15) comes from the work of Aamo et al. [21] on the control of mixing in pipe flows. In [21] it was shown using an energy-based argument that a similar strategy achieves an optimal enhancement of flow quantities related to mixing. The effect on mixing was confirmed by simulations. While the control strategy in [21] has inspired (14) and (15), the analogy is not complete. In [21] the 3-D pipe flow is controll using actuators and sensors distributed on the (2-D) wall of the pipe. In the jet flow problem here, which is 2-D, point actuation and sensing are employed (i.e. 0-D). Due to the 'underactuated' nature of the problem we consider that the use of a delay (or some more complex compensator dynamics) is essential. We demonstrate that a delay is sufficiently capable of significantly affecting the flow, although more complex, fully theoretically justified control strategies, might be even more effective.

4 Simulation results

4.1 Uncontrolled jet

Simulation results for the jet flow without a controller at a Reynolds number $Re_D = 100$ are used to validate the code

relative to theory and previous works, and serve as the base case. The jet's half-width growth rate, centreline velocity decay rate and normalised velocity profiles of the statistical data at t=1000 after the simulation is initiated, are examined. The jet's half-width is found to grow linearly and the squared ratio of the centreline velocity to the exit centreline velocity also has a linear growth along the streamflow direction of the jet beyond the potential core. The half-width growth rate and centreline velocity decay rate can be described by linear functions:

$$\delta_{1/2}(x_1) = C_{\delta}(x_1 + x_{\delta}) \tag{16}$$

$$\left(\frac{U_0}{u_c(x_1)}\right)^2 = C_u(x_1 + x_u) \tag{17}$$

where $\delta_{1/2}$, the half-width, is the distance between the centreline and the point where the mean streamflow velocity is half that of the centreline velocity u_c , C_δ and C_u are the growth and decay rates, and x_δ and x_u are the virtual origins. The virtual origin is a point source located upstream of the nozzle exit where a theoretical jet is initiated. The theoretical jet initiated from this virtual origin will have the same momentum as the actual momentum of a real jet discharged at the nozzle exit, and will produce a self-similar velocity profile beyond the potential core.

The half-width growth and centreline velocity decay of the current results are plotted in Figs. 2a and 2b, respectively, along with plots of the least-square fit linear function. The linear relation of the growth and decay rate with the stream coordinate is obvious. The slopes and virtual origins of (16)–(17) obtained from this work and previous experimental and numerical works are also listed in Table 1 for comparison. The current results show a slower growth rate and virtual origin that is further upstream for the halfwidth, whereas the decay rate and virtual origin fall in the nominal range for centreline velocity. One should keep in mind that the initial condition at the jet nozzle exit has long lasting effects on the jet flow development downstream. The velocity profile at the jet nozzle in our study is a well developed channel flow which gives almost no near field and the jet flow directly enters the transient field. Therefore, a virtual origin that is further upstream and a slower growth rate is expected.

The normalised stream direction velocity and transverse velocity are plotted against a normalised coordinate ξ between $x_1 = 5$ to $x_1 = 20$ in Figs. 2c and 2d, respectively. The normalised coordinate ξ is a cross-stream similarity variable defined as the normal coordinate x_2 as a function of the half-width $\delta_{1/2}(x_1)$. In the fully developed region, the profiles of the normalised velocity in the streamflow direction u_1/u_c at different streamflow locations, plotted against ξ , collapse onto a single curve. The profiles of velocity in the normal direction u_2/u_c also become self-similar with little inconsistency due to the effect of the 2-D simulation. Despite the small deviations in the half-width growth, the current results agree with the theoretical and experimental results. The vorticity plot and streaklines of an uncontrolled jet at t = 500, shown in Fig. 3a and Fig. 4a, confirm that the dominant unstable mode is the flapping mode.

4.2 Controlled jet

Two closed-loop controlled cases with the same feedback gain but different sensor configurations, one with a sensor downstream at $x_1 = 5$ and the other with a sensor at the jet exit with a delay of $\tau = 15$, are presented to demonstrate the effectiveness of the control laws (14) and (15) by comparing them with the uncontrolled case. Due to the feedback-loop,

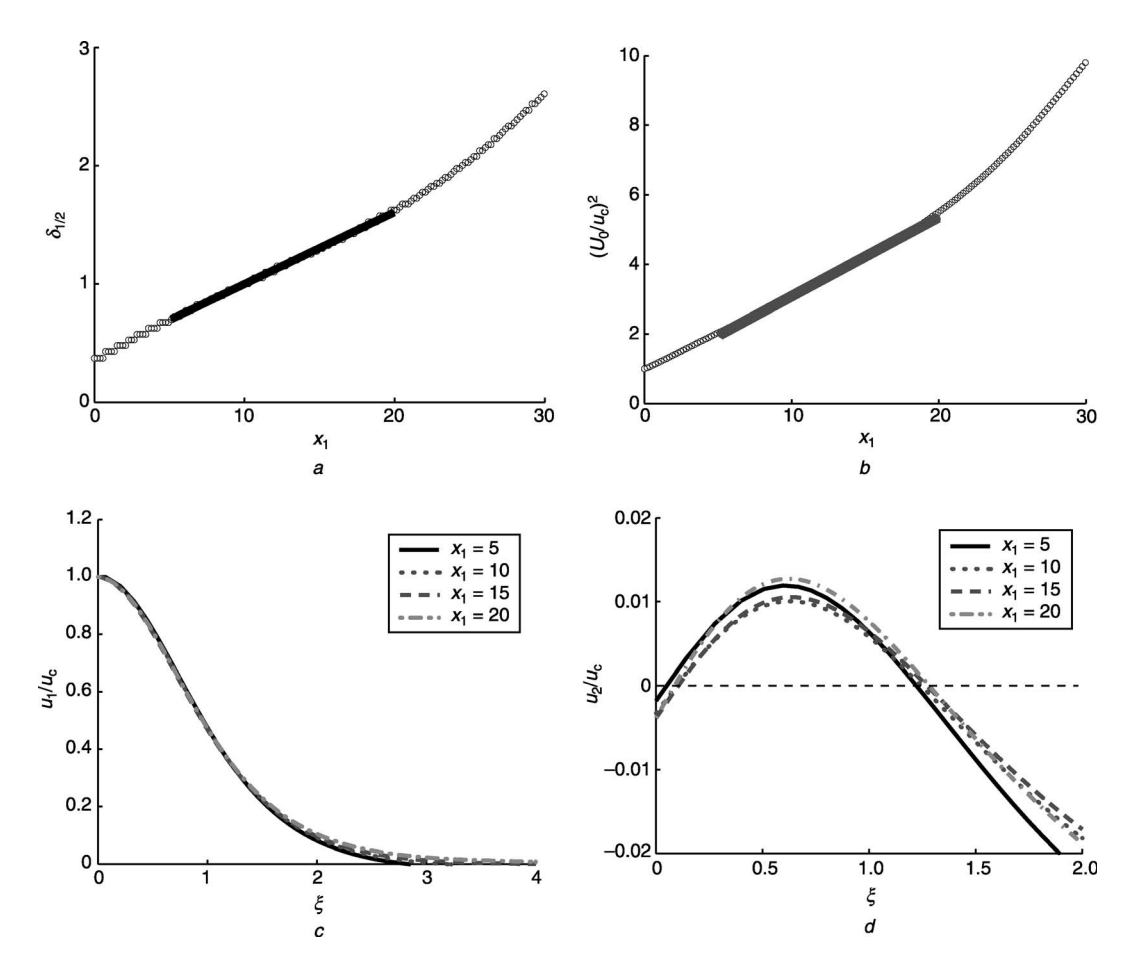


Fig. 2 Self-similarity profile

- a Half-width
- b Centreline velocity
- c Mean stream direction velocity
- d Mean normal velocity

Table 1: Comparison of the jet's half-width growth rate and centreline velocity decay rate

	Re	$oldsymbol{\mathcal{C}}_{\delta}$	$ extbf{ iny X}_{\delta}$	C_u	x_u
Present result	100	0.061	6.36	0.227	3.58
Sarkar et al. [6]	3000	0.092	2.63	0.201	1.23
Ramaprian and Chandrasekhara [5]	1600	0.112	1.00	0.093	1.60
Hussain and Clark [3]	32 550	0.118	2.15	0.123	4.47
Miller and Comings [4]	17 800	0.072	1.57	0.181	4.20

the actuation eventually falls into a limit cycle with a frequency determined either by the sensor location or by the time delay. Also shown here is an open-loop controlled case with sinusoidal forcing:

$$U_1(t) = -U_2(t) = A\sin(\omega t) \tag{18}$$

where ω is the forcing frequency and A its amplitude. The presented open-loop case has a forcing frequency $\omega = 0.06\pi$ which is the same as the frequency of the limit cycle obtained with feedback with a delay of $\tau = 15$. A detailed comparison of other values of sensor location, time delay and open-loop forcing frequency can be found in [18], and quantification between these control laws will be discussed in Section 5.

The vorticity fields of controlled cases at t = 500 are shown in Figs. 3b-3d. These controllers obviously alter the jet flow from the uncontrolled case by generating vortices of different sizes and spreading pattern. Whereas the controller

with a sensor with a single delay generates vortices more regularly with a narrower spreading pattern, the controller with a sensor downstream gives a wider spreading pattern. The streaklines of the uncontrolled and controlled cases at t = 500 shown in Figs. 4a and 4b suggest that smaller vortices draw more massless particles into the vortex core due to more rapid rotation and this benefits the fluid particle mixing.

Similarities between the two different sensor schemes can be observed. The controller with a sensor at the nozzle exit without any delay has very little effect on jet development downstream; the controller-induced instability is too weak and will quickly decay if the feedback gain is low, however, the controller will generate a rapid bang-bang action once the feedback gain is tuned too high. For the controller with a sensor downstream, a minimum distance from the nozzle exit to the sensor is required so that the vortices can be produced, and this minimum distance is a function of the Reynolds number

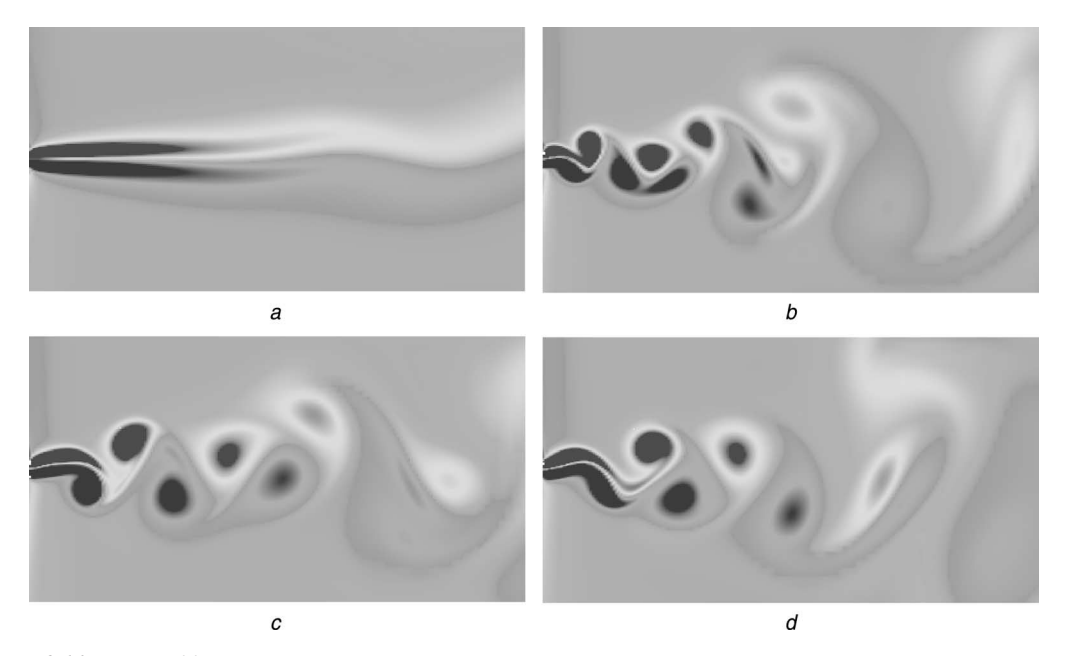


Fig. 3 *Vorticity fields at t* = 500a Uncontrolled jet $b x_1 = 5$ $c \tau = 15$

d Open-loop forcing

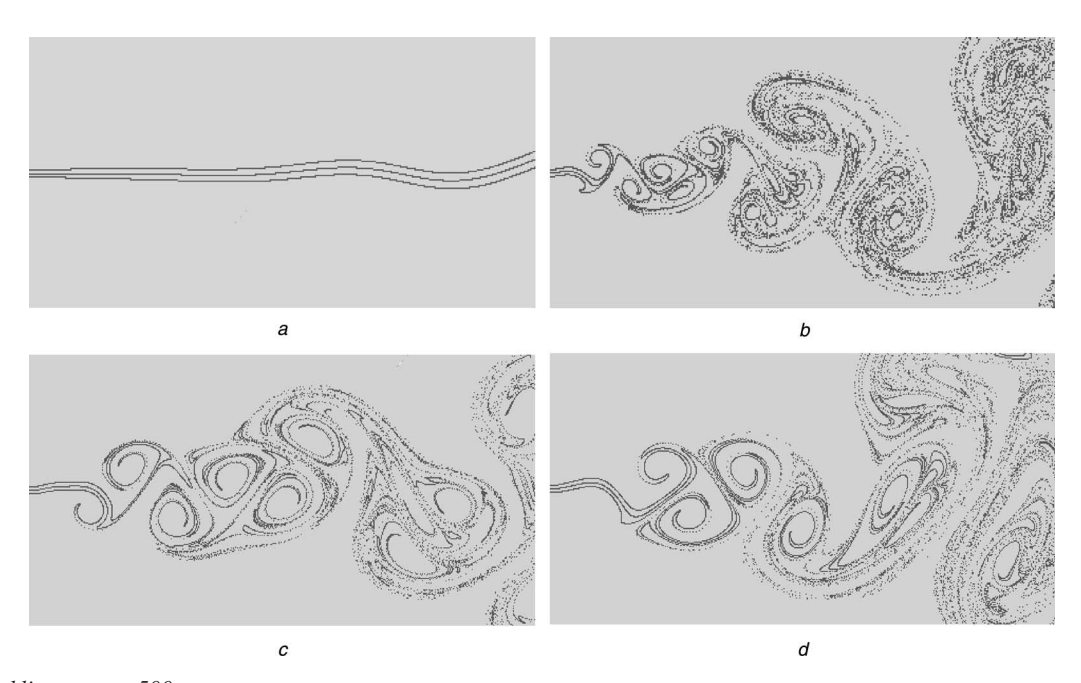


Fig. 4 *Streaklines at* t = 500a Uncontrolled jet

 $b x_1 = 5$

 $c \tau = 15$

d Open-loop forcing

of the flow. A minimum feedback gain is also essential to sustain the instability introduced by the actuator and to break it up into vortices. For the control law with a sensor at the jet exit with a delay, in order to be able to generate vortices and to maintain this generation, the delay and feedback gain must meet minimum demand values, too. Even although these similarities are observed, no direct relation between the sensor location and the time delay length for these two sensor configurations is available. For the downstream sensor configuration the generated vortices go through different spatial developments and various convection velocities before reaching the sensor. This feedback-loop involves the uncertainty in the spatial development. On the other hand, the sensor at the exit is less influenced by the downstream spatial development of the flow.

By carefully tuning the feedback gain and delay, a control law with a delayed sensor can produce a very similar flow field to the one generated by the controller with a downstream sensor. The underlining mechanism for this exchange between the two types of sensors is that the timescale provided by the delay can replace the lengthscale provided by the sensor location. Measuring the pressure difference at the jet nozzle exit is more practical than taking a measurement downstream, and we shall concentrate on the controllers with delayed sensors.

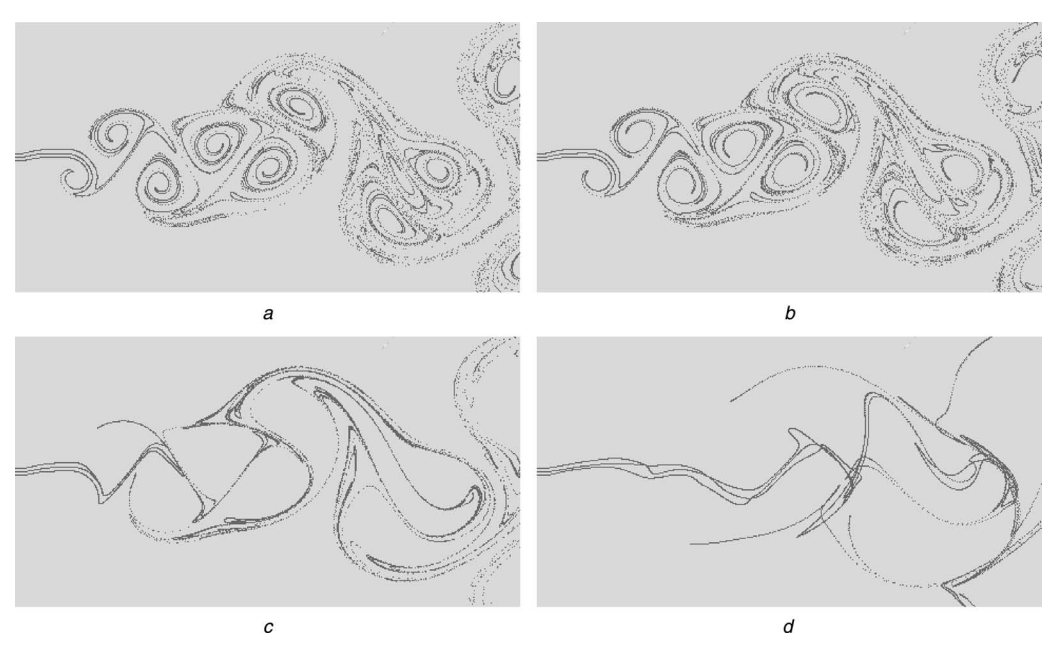


Fig. 5 Particle distribution of controlled jet (sensor with delay $\tau = 15$)

a Streaklines

b St = 0.1

c St = 1

d St = 10

4.3 Particles with mass

The distribution of particles with mass is an essential tool to study the gas-particle jet flow. The closed-loop controlled case using the sensor at the exit with a delay $\tau=15$ is used to show the results of particle mixing. The distribution of particles with different Stokes numbers at t=500 is shown in Fig. 5 along with the streaklines. Whereas the light particles are attracted into the vortical structure and transported by the vortices, the heavy particles are not so transported. This result is consistent with the observations of [19] and [22].

The light particles with St = 0.1 closely follow the fluid motion acting like a tracer. The distribution of particles

almost duplicates the streaklines except that fewer particles are attracted into the eddy cores. Since the particle mass is considered in the evolution, the additional drag force slows down the particle motion and the particle does not follow the fluid motion instantaneously.

Particles with a unity Stokes number tend to centrifuge out of the vortex cores and concentrate on the peripheries of the vortical structures. The response time of the medium particles with St = 1 is too slow to follow the large velocity gradient temporally and spatially inside the vortices. Thus, they are radiated out from the high-vorticity region eddy core and accumulate between vortices. This is also called a demixing phenomenon by Crowe *et al.* [19].

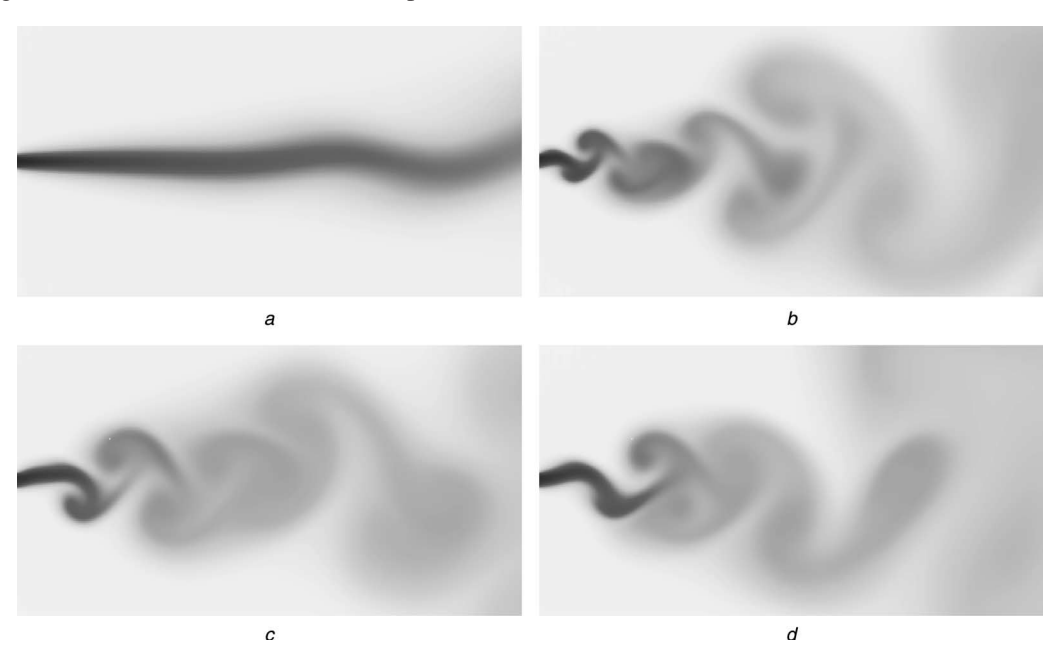


Fig. 6 Scalar field at t = 500a Uncontrolled jet b $x_1 = 5$ c $\tau = 15$

d Open-loop forcing

For a large Stokes number, the inertia of heavy particles is too great to let the carrier fluid significantly influence the particle motion. The particles travel a long distance before the vortices start to have any influence on them. A small fraction of the medium particles in the far field are centrifuged by the radial force of the strong vortices, but most of the particles are directly convected downstream but are not dispersed by the vortices. Once a heavy particle is pushed by the surrounding fluid, it will not respond fast enough to any subsequent opposing velocity vectors due to its long momentum response time. This slow reaction of the heavy particles to the fluid motion leaves the traces of vortex passage shown in Fig. 5d in which particles are pushed outwards from the eddies and slowly convected downstream by subsequent fluid motion.

The closed-loop controller has shown a promising result on the mixing enhancement of particles with mass, yet the performance degrades as the particles become heavier.

4.4 Passive scalar

The scalar field for an uncontrolled and a controlled jet obtained using different control laws is shown in Fig. 6. The controlled jet evidently has a better mixed scalar field than the uncontrolled jet. The scalar dispersion is found to be mostly carried out by the rotation, convection and spreading of generated vortices. A smaller vortex with a strong vorticity seems to constrain the diffusion of the passive scalar. On the other hand, wider vortex spreading helps to convect and transport the scalar field. Once the vortex rings are convected downstream and expanded, the diffusion effect becomes more apparent as the intensity of the vorticity subsides.

The diffusivity of the studied scalar is comparable to that of the carrier fluid if the Schmidt number is set to unity. Thus, the evolution of the scalar is mainly dominated by the convection terms. This can be observed by comparing the scalar field plots with the vorticity plots such that the concentration of the scalar is consistent with the vortical structure.

5 Discussion

Without the length separation provided by the sensor downstream or time separation by the sensor at the nozzle exit with a delay, the controller produces insufficient influence on the jet. Another important factor is the amplitude of the actuator. The interval between an actuator switching directions is determined by the sensor, but the feedback gain decides whether the perturbation induced by the actuation will grow strong enough to break up into a vortex or will just subside. The time histories of a control signal for the single delay case $\tau=15$ with two different feedback gains, K=15 and 10, upto t=500, are plotted in Fig. 7a. With a feedback gain higher than the minimum requirement $\simeq 13$, the actuation grows exponentially until it reaches saturation and it then enters a limit cycle; with a feedback gain lower than the minimum requirement, the control decays and provides insufficient perturbation to the flow. The control change rate is plotted in Fig. 7b, and it is limited to a maximum value of $0.2U_0$.

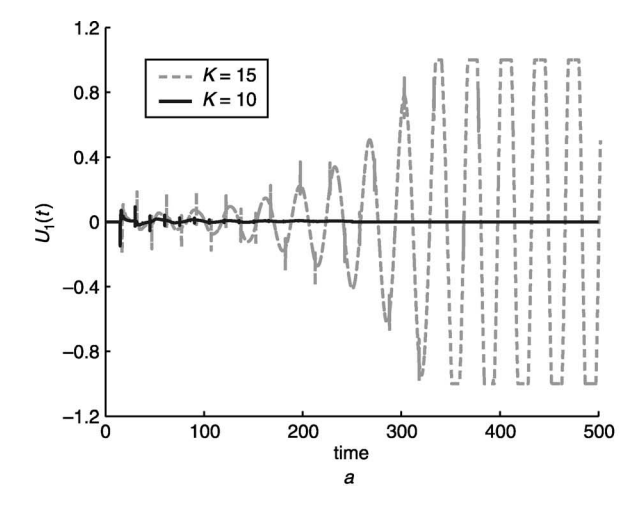
A measure of mixing is necessary to quantify the effectiveness of the presented control law. Several diagnostic tools for finite-time mixing are available. The notions of finite-time stable and unstable manifolds, were introduced and applied in [23–25] where as [26] and [28] examined the mixing property using statistical properties. (Please see these references for more details.) In this study, a probability function similar to the one used in [20, 21] is constructed for both the particle distribution and scalar field.

The physical domain is divided into N boxes, and the probability P of a box holding the number of particles n_p or scalar value n_s in a certain range at time t is calculated by:

$$P_{p}(t) = \frac{1}{N_{p}} \sum_{i=1}^{N_{p}} \text{eval}(25 \le n_{p}^{i}(t) \le 75)$$
 (19)

$$P_{s}(t) = \frac{1}{A} \sum_{i=1}^{N_{s}} \text{eval}(0.25 \le n_{s}^{i}(t) \le 0.5) \times a^{i} \quad A = \sum_{i=1}^{N_{s}} a^{i}$$
(20)

where the subscripts p and s denote particle and scalar, respectively, the superscript i indicates the ith box, eval is a function that returns value of one if n_p^i or n_s^i falls between the lower and the upper limit, A is the total area in the physical domain, and a^i is the area of the local cell. The box size for the particle probability is uniform and has a unity area; the box size for a scalar field is not uniform and is consistent with the computation cell. If the number of particles (or the scalar value) in a cell is above the upper limit, the mixture is too dense; below the lower limit it is too thin, and in-between it is considered well mixed. One should



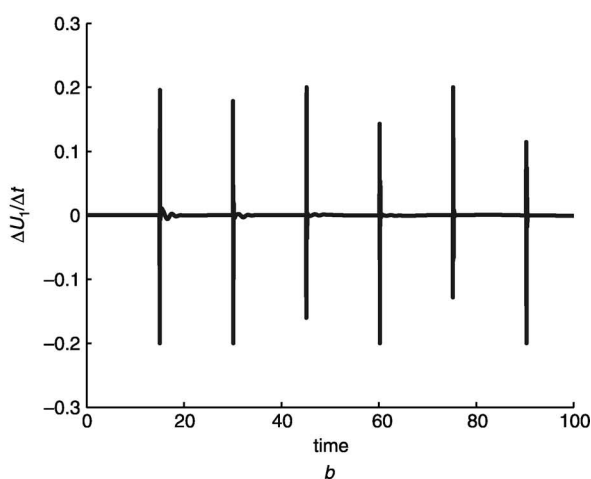


Fig. 7 Control signal and control change rate of controlled jet ($\tau = 15$)

a Control signal

b Control change rate

note that this probability function is a function of time and would be altered if the lower or upper bounds are changed. The choice of these limits which defines the mixing quality is application dependent but this topic will not be further discussed.

In [18], closed-loop controllers based on (14) and (15) with various values for x_1 and τ were compared. For the case with the downstream sensor, (14), the values $x_1 = 0, 2.5, 5$, 7.5 and 10 were tested, and $x_1 = 5$ was found to give the best performance based on the metric defined in (19) for massless particles. Similarly, for the case of a sensor at the nozzle exit with a delay (15), the values $\tau = 0, 5, 10, 15, 20$ and 25 were examined, and $\tau = 15$ was found to give the best result. A comparison between these two specific closedloop controllers and open-loop forcing with same frequency of the limit cycle of $\tau = 15$ is made through (19) and (20). The probability functions of the scalar field and particles with a mass for both uncontrolled and controlled cases are plotted in Fig. 8. Since the evolution of light particles (St = 0.1) is very similar to the massless particles, a comparison of probability functions for their streaklines will not be presented.

The controlled cases show a significant improvement in scalar mixing over the non-controlled case by doubling (downstream sensor and open-loop forcing) and tripling (sensor at nozzle exit with a delay) the probability function value in the quasi-steady-state conditions. The bumps observed in the probability function curves are caused by

the vortex structures leaving the domain, and this confirms that the convection and expansion of a vortex is a significant contributor to the scalar mixing. The delayed sensor case shows the best performance among these three controlled cases. The holding interval of the actuation for the delayed sensor case (see Fig. 7) helps to produce stronger vortices and to let the vortex penetrate into the downstream. This strong intensity and penetration helps to keep the scalar in the nominal range. The sensor downstream case or openloop forcing, on the other hand, generates a wider spreading pattern or weaker vortices such that the diffusion effect becomes dominant but dilutes the scalar beyond the lower limit.

The controlled jet flows also show a better mixing quality for particles with mass, but the effectiveness of the controller decreases as the Stokes number of the particle increases. For light particles St = 0.1, the closed-loop controllers produce a higher probability function value than the open-loop forcing, and the value is three times as great as the one of the uncontrolled case in the quasi-steady-state conditions. For medium particles St = 1, the closed-loop controlled cases still show a better performance than the open-loop forcing case and the value of the probability function is around double that of the uncontrolled case at the end. For heavy particles St = 10, all controlled cases show no improvement on mixing from the base case. This is in contrast to the particle distribution shown in Fig. Sd in which the particles are very different from the uncontrolled

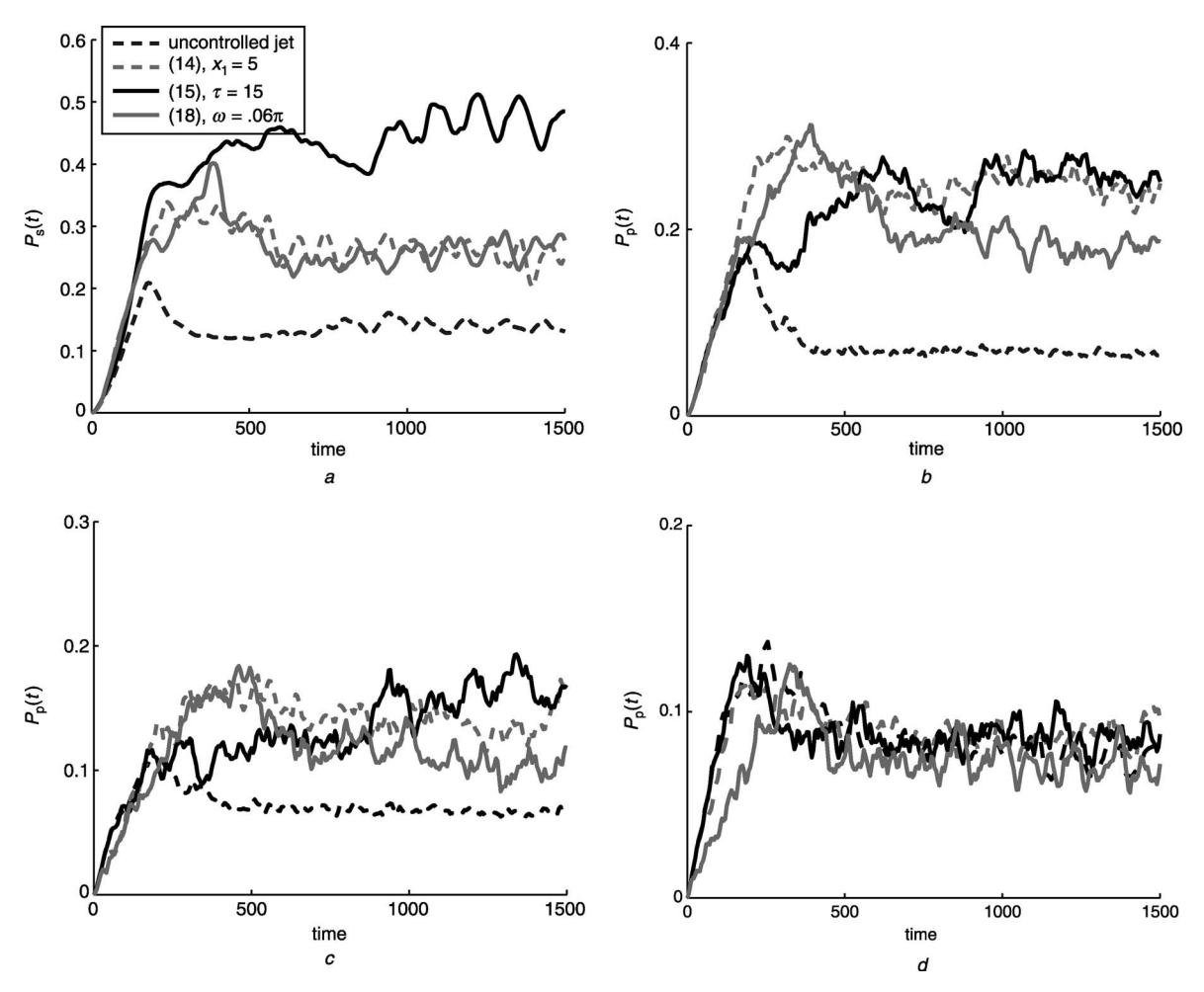


Fig. 8 Probability function of scalar field and particles with different Stokes numbers

a Scalar field

b St = 0.1

c St = 1

d St = 10

case. One should note that a lower limit will increase the value of the probability function. Apparently, a controller that acts solely on the carrier phase has a very limited effect on the path of heavy particles. A separate controller that acts directly on the particles is necessary to enhance the mixing for heavier particles.

6 Conclusions

The formation of vortices and their interactions govern the entrainment and mixing in jet flows. The perturbation initiated at the nozzle exit is an essential phenomenon and is responsible for vortex break up downstream, and this is in turn is the key to mixing enhancement. The closed-loop controllers developed here successfully produce a vortex generation pattern that enhances the overall mixing. Whereas the configuration of a downstream sensor provides an idea for a control law, the length scale obtained from the sensor location can be used as the delay in the more feasible configuration of a sensor at the nozzle exit.

Whereas all the controlled cases presented here show promising results on mixing as evidenced by the snapshots taken at the vorticity field and streaklines, the closed-loop controller with a sensor at the nozzle exit with a delay gives the best mixing result measured in terms of a probability function in the scalar field and particles with a mass. The performance of a controller should not be decided by a single criterion and one should take into account many aspects, e.g. vorticity field, streaklines, distribution of particles or scalar, and/or probability functions of particles or scalar. The performance criterion is application dependent, and fine tuning of the control parameters, delay length and feedback gain, is necessary to have an effective vortex generation pattern that leads to a desired mixing quality. Extremum seeking [28] is one option available for such nonmodel-based optimisation/tuning.

In Section 5 we compared the performance of our feedback strategy with both the uncontrolled flows and with those resulting from open-loop forcing at the frequency of vortex shedding. Since, in steady-state conditions, the feedback controller results in a periodic actuation signal, one can argue that its effect is not significantly different from the effect of periodic open-loop forcing. This argument could be supported with the results of the mixing experiments where the open-loop forcing is not significantly less successful than the feedback strategies. However, one should not forget that the open-loop strategy requires an exact knowledge of the frequency of limit cycling achieved by the feedback controller, whereas the feedback controller enters such oscillation 'on its own'. Whereas a well tuned open-loop controller forces certain modes of the flow, the feedback controller destabilises them, it becomes a part of the dynamics of those modes.

7 Acknowledgments

This work was supported by the Taiwan (Republic of China) Navy, the Office of Naval Research, the Air Force Office of Scientific Research, and the National Science Foundation.

8 References

- Schlichting, H., and Gersten, K.: 'Boundary layer theory' (Springer-Verlag, 2000)
- Grinstein, F.F., Gutmark, E.J., Parr, T.P., Hanson-Parr, D.M., and Obeysekare, U.: 'Streamwise and spanwise vortex interaction in an axisymmetric jet. A computation and experimental study', Phys. Fluids,
- 1996, **8**, (6), pp. 1515–1524

 3 Hussain, A.K.M.F., and Clark, A.R.: 'Upstream influence on the near field of a plane turbulent jet', *Phys. Fluids*, 1977, **20**, (9), pp. 1416–1426 Miller, D.R., and Comings, E.W.: 'Static pressure distribution in the
- free turbulence jet', *J. Fluid Mech.*, 1957, 3, pp. 1–16 5 Ramaprian, B.R., and Chandrasekhara, M.S.: 'LDA measurements in
- plane turbulent jets', Trans. ASME, I. J. Fluids Eng., 1985, 107, pp. 264-271
- 6 Stanley, S.A., Sarkar, S., and Mellado, J.P.: 'A study of the flow-field evolution and mixing in a planar turbulent jet using direct numerical simulation', *J. Fluid Mech.*, 2002, **450**, pp. 377–407
- Paschereit, C.O., Wygnanski, I., and Fiedler, H.E.: 'Experimental investigation of subhar monic resonance in an axisymmetric jet',
- J. Fluid Mech., 1995, **283**, pp. 365–407 8 Thomas, F.O., and Prakash, K.M.K.: 'An experimental investigation of the natural transition of an untuned planar jet', Phys. Fluids A, 1991, 3,
- pp. 90–105

 9 Freund, J.B., and Moin, P.: 'Mixing enhancement in jet exhaust using fluidic actuators: direct numerical simulations'. Proc. of FEDSM98, ASME, New York, 1998
- 10 Gutmark, E.J., and Grinstein, F.F.: 'Flow control with noncircular jets', Annu. Rev. Fluid Mech., 1999, 31, pp. 239-272
- 11 Gutmark, E.J., Parr, T.P., Wilson, K.J., and Schadow, K.C.: 'Active control in combustion systems with vortices'. Proc. 4th IEEE Conf. on Control Applications, 1995, pp. 679–684
 12 Parekh, D.E., Kibens, V., Glezer, A., Wiltse, J.M., and Smith, D.M.:
- 'Innovative jet flow control: mixing enhancement experiments'. Paper 96-0308 presented at the AIAA Conf., 1996

 13 Lardeau, S., Lamballais, E., and Bonnet, J.-P.: 'Direct numerical
- simulation of a jet controlled by fluid injection', J. Turbul., 2002, 3,
- p. 002
 14 Suzuki, H., Kasagi, N., and Suzuki, Y.: 'Active control of an actuators', axisymmetric jet with distributed electromagnetic flap actuators',
- Exp. Fluids, Fluid Dyn., 2004, 36, pp. 498–509
 Akselvoll, K., and Moin, P.: 'Large eddy simulation of turbulence confined coannular jets and turbulent flow over a backward facing step', Report TF-63, Thermosciences Division, Dept. of Mech. Eng., Stanford University, Stanford, CA, 1995
- 16 Bewley, T.R., Moin, P., and Teman, R.: 'DNS-based predictive control of turbulence: an optimal benchmark for feedback algorithms', J. Fluid
- Mech., 2001, 447, pp. 179–225 Colonius, T., Lele, S.K., and Moin, P.: 'Boundary conditions for direct computation of aerodynamic sound generation', AIAA J., 1993, 31, (9),
- pp. 1574–1582 Yuan, C.-C.: Yuan, C.-C.: 'Control of jet flow mixing and stabilization'. PhD dissertation, University of California at San Diego, San Diego, CA, 2002
- 19 Crowe, C.T., Sommerfeld, M., and Tsuji, Y.: 'Multiphase flows with
- droplets and particles' (CRC Press, 1998)

 20 Aamo, O.M., and Krstić, M.: 'Flow control by feedback' (Springer, 2002)
- Aamo, O.M., Balogh, A., and Krstic, M.: 'Optimal mixing by feedback in pipe flow'. Presented at the IFAC World Congress, Barcelona, 2002 Loth, E.: 'Numerical approaches for motion of dispersed particles,
- droplets and bubbles', Prog. Energy Combust. Sci., 2000, 26,
- arropiets and bubbles, Frog. Energy Combust. Sci., 2000, 20, pp. 161–223
 Haller, G., and Poje, A.C.: 'Finite time transport in aperiodic flows', Physica D, 1998, 119, pp. 352–380
 Haller, G.: 'Finding finite-time invariant manifolds in two-dimensional velocity fields', Chaos, 2000, 10, (1), pp. 99–108
 Haller, G., and Yuan, G.: 'Lagrangian coherent structures and mixing in the dimensional turbulones', Physica D, 2000, 147, pp. 352–370
- two-dimensional turbulence', *Physica D*, 2000, **147**, pp. 352–370

 26 D'Alessandro, D., Mezić, I., and Dahleh, M.: 'Statistical properties of
- 20 Alessandro, D., McZik, I., and Dainell, Mr. Statistical properties of controlled fluid flows with applications to control of mixing', Syst. Control Lett., 2002, 45, pp. 249–256
 27 Mezić, I., and Narayanan, S.: 'Overview of some theoretical & experimental results on modeling and control of shear flows'. Proc. 39th IEEE Conf. on Decision and Control, Sydney, Australia, 11–15 December 2000
- 28 Krstic, M., and Wang, H.-H.: 'Stability of extremum seeking feedback for general dynamical systems', Automatica, 2000, 36, pp. 595-601